Sensors and Materials, Vol. 37, No. 8 (2025) 3515–3529
MYU Tokyo

S & M 4134

Performance Enhancement of Microbial Fuel Cells Using Graphene-coated Stainless Steel Mesh Anodes via Electrophoretic Deposition

Wei-Hsuan Hsu* and Zih-Yu Lin

Department of Mechanical Engineering, National United University, No. 2, Lienda, Miaoli 360302, Taiwan

(Received November 5, 2024; accepted August 8, 2025)

Keywords: microbial fuel cell, stainless steel mesh, electrophoresis deposition, graphene, Taguchi method

Microbial fuel cells (MFCs) utilize sewage and bacteria to generate electricity with low pollution, yet their power output remains insufficient for practical applications. To address this, in this study, we focus on the energy harvester technology of MFCs, specifically the micro/nanostructure fabrication of nanomaterials used for anode electrodes in energy collection. Electrophoretic deposition (EPD) is employed to fabricate a uniform graphene film on stainless steel mesh anodes, aiming to enhance the energy harvesting efficiency of MFCs. EPD offers advantages such as large-area deposition, shape flexibility, and tunable film compactness through parameters like voltage, time, and suspension composition. The Taguchi method was used to analyze the impact of these parameters. Experimental results show that the EPD-coated graphene anode significantly boosts power output, raising the maximum power density from 0.70 mW/m² (without modification) to 5.65 mW/m², an eightfold increase. This underscores the effectiveness of the micro/nanostructured electrode modification approach for energy harvesting applications.

1. Introduction

As technology has evolved, human society has become increasingly prosperous and life has become more convenient. People consume considerable energy in their daily lives. However, the waste gas generated by combusting fossil fuels is increasingly detrimental to the environment; it depletes the ozone layer, causes climate abnormality, creates air pollution, and indirectly affects the health of human beings and other creatures. Thus, the development of green energy and technology has garnered increasing attention. Researchers worldwide have been dedicated to the development of green energy to prevent energy crises. Biomass energy is a type of renewable energy that is created by microbes in animal waste and agricultural residue. By using biomass energy, which turns waste into resources, the efficiency of resource application can be improved.[1] The development of biomass fuel may mark the turning point of the energy crisis.

*Corresponding author: e-mail: whhsu@nuu.edu.tw
https://doi.org/10.18494/SAM5459

ISSN 0914-4935
https://myukk.org/

Among the numerous green energy technologies, microbial fuel cells (MFCs) with water as the final product have the advantages of low cost and little pollution production.

In MFCs, microbial metabolism is employed to generate electricity. Because waste water commonly contains multiple strains of bacteria, it can be collected and used as an MFC electrolyte for the generation of electricity.[2] Therefore, MFCs can reduce industrial and agricultural waste gas emissions, the cost of transporting and disposing sewage, and the damage to the environment caused by industrial production processes.[3] The number of investigations on MFC power generation efficiency has been increasing recently. Because many factors may affect this efficiency and numerous types of electrode are available, many electrode modification methods have not yet been discussed. Thus, there is scope for considerable improvement in the MFC field.

The factors affecting the performance of an MFC are innumerable. Common study topics include electrode materials, electrode intervals, bacterial strains, and anodic solutions (the fuel). Anode characteristics were discovered to have the most notable effect on the MFC power generation efficiency.[4] An MFC anode base material must generally have favorable conductivity, high structural strength, and high corrosion resistance if the overall power generation efficiency is to be high. Stainless steel base materials have excellent conductivity and low cost [e.g., stainless steel mesh (SSM),[5–7] stainless-steel foam,[8] stainless-steel felt,[9,10] stainless steel fiber felt,[11,12] and carbon cloth]. The development of nanomaterials continues, and these materials are garnering increasing attention because of their effectiveness in reducing electrical resistance and increasing output current and electron transport rate.[4,13–19] The combination of such nanomaterials with a relatively inexpensive stainless steel base material is offering many opportunities for novel MFC development. Therefore, the fabrication processes used for the surface modification of SSMs merit further exploration.

Electrophoretic deposition (EPD) is a technique in which charged particles suspended in a stable colloidal solution are driven through the liquid by an electric field and deposited onto an oppositely charged conductive substrate.[20] This process yields the desired material or device. EPD facilitates the fabrication of a diverse array of structures, ranging from traditional to advanced materials, including nanometric thin films, films less than 1 mm thick, porous scaffolds, and highly compact coatings.[21] An *et al.* utilized EPD to prepare graphene oxide coatings. Their research demonstrated that the EPD process can create layered graphene oxide coatings, with the flakes covering and stacking upon one another.[22] Furthermore, EPD has proven effective in enhancing MFC performance through electrode modification. Sayed *et al.* used EPD to coat carbon brush anodes with reduced graphene oxide, increasing the power density from 33 to 381 mW/m² by improving electron transfer.[14] Choi *et al.* fabricated Ni-based nanocatalysts on carbon felt via EPD, with the power density of Ni/NiOx electrodes reaching 1630.7 mW/m², a 400% increase compared with commercial Pt/C.[15] Khajeh *et al.* applied EPD to deposit CuO/ZnO nanoparticles onto graphite cathodes and achieved 51.84 mW/m², which is 2.74 times higher than that of unmodified electrodes under visible light.[16] The results of these studies demonstrate the potential of EPD as a low-cost, scalable method for developing high-performance MFC electrodes.

This study is focused on energy harvester technology, specifically the micro/nanostructure fabrication of nanomaterials used for anode electrodes in energy collection. Referring to previous studies on applying EPD in MFCs, we explore the use of SSM, a conductive and readily available material, as the anodic base material for MFCs, aiming to enhance its energy harvesting performance. Graphene, known for its excellent electrical and structural properties, was deposited onto the SSM surface via EPD, a method suitable for fabricating uniform micro/nanostructured films. Given the increasing maturity of graphene processing techniques, EPD offers a controllable and scalable approach to electrode modification. To further optimize the effectiveness of the graphene-based enhancement, the Taguchi method was applied to systematically evaluate the effects of EPD parameters on the structure and performance of the modified electrodes. This approach highlights the potential of integrating nanomaterials and micro/nanofabrication techniques in advancing sustainable energy harvesting applications.

2. Materials and Methods

2.1 EPD process and materials

The preparation procedure of the graphene suspension used in the EPD process is described below. After deionized water and ethanol were mixed in a ratio of 1:1, graphene powder (Enerage Inc., Taiwan) was added to the mixture to obtain graphene suspensions with concentrations of 0.01, 0.02, and 0.03 wt%. Then, 0.5 g of magnesium nitrate was added to the suspensions, which were subsequently oscillated for 1 h by using an ultrasonic oscillator to evenly distribute the graphene powder in the solutions. Magnesium nitrate was added as an adsorbent to make the graphene suspensions weakly acidic, enabling the adsorption of graphene on the cathode end of the EPD system during the EPD process.

Figure 1 presents a schematic of the EPD system, which had a glass tank of 150 × 50 × 180 mm. An 85 × 85 mm^2 316 SSM (400 mesh size, E Shie Zong Co., Ltd., Taiwan) electrode was fixed in place in the EPD system to act as its cathode. Likewise, an SSM of the same size was fixed in place to act as the anode. The two electrodes were fixed using polyactide (PLA) clamps, which maintained the electrodes' flatness. The electrode interval was 5 mm. We adjusted four parameters—the DC voltage, deposition time, deposition temperature, and graphene concentration—to control the density of graphene adhered onto the SSM surface.

The SSM used as the anode in the MFC system was coated with graphene. To strengthen the adhesion between graphene and SSM, the graphene-covered SSM was presintered at 350 °C for 1 h and heat-treated in a tube furnace at 650 °C for 1 h to create carbon–metal bonds between graphene and electrode base material.

2.2 MFC construction and system setup

The effectiveness of the EPD-treated SSM anodes was demonstrated by the improvement in the power generation of the MFC. Figure 2 illustrates the single-chamber MFC used in the experiment. As shown in Fig. 2(a), the air-cathode MFC has a rectangular shape with a

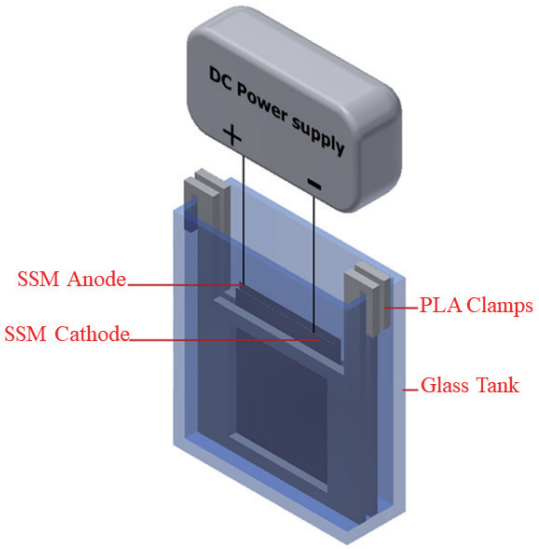

Fig. 1. (Color online) Schematic of the EPD system.

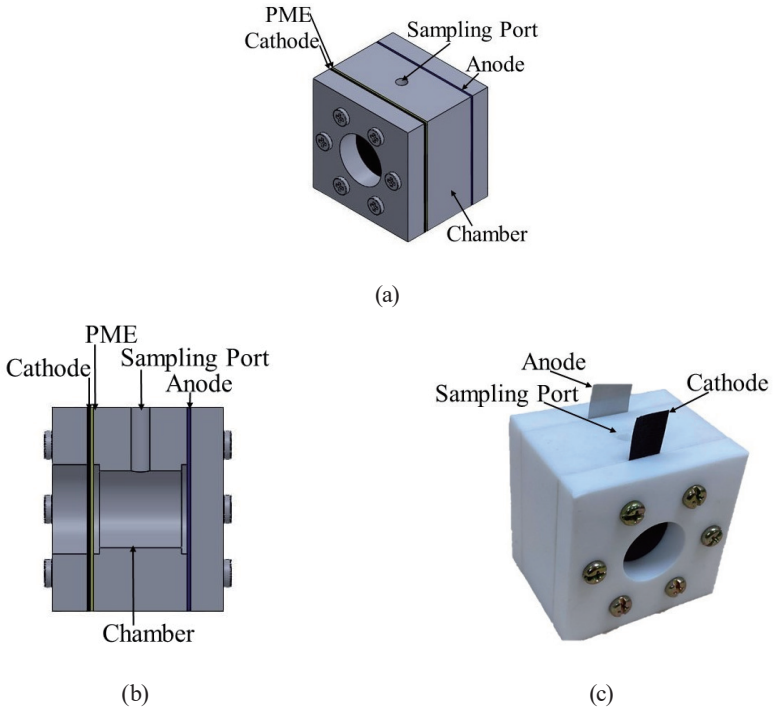

Fig. 2. (Color online) (a) Schematic, (b) cross-sectional view, and (c) actual appearance photograph of the single-chamber MFC used in the experiment.

cylindrical through-hole that measures 24.5 mm in diameter and 30 mm in length, resulting in a total reactor volume of approximately 14.14 mL. Figure 2(b) presents a cross-sectional view that reveals the electrode configuration. Figure 2(c) shows the appearance of the single-chamber

MFC once it has been assembled. The chamber of the single-chamber MFC is made from Teflon, and screws and O-rings are used to seal the anode tank and secure the electrodes. The SSM anode is fixed on the closed side of the cylindrical chamber. A proton-exchange membrane (PEM, Nafion 117, Dupont Co., USA) and a carbon cloth cathode (W1S1010, CeTech Co., Ltd., Taiwan) are fixed on the air side of the cylindrical chamber.

In this study, we use the same microorganisms and anode solution as described in our previous papers.[4,19] To accurately assess the effect of EPD treatment on MFC performance and minimize experimental variability, *Escherichia coli (E. coli)* HB101 was employed as the biocatalyst for energy conversion. HB101 was cultured in Luria–Bertani (LB) medium at 37 ℃ for 9 h. Methylene blue was used as an electron mediator to transfer the liberated electrons to the anode surface.[23] Glucose acted as the fuel, and the anolyte was prepared by dissolving 6.9 g of glucose powder and 0.1 g of methylene blue powder in 102.5 g of HB101 solution.

2.3 Taguchi method experimental design

The Taguchi method is widely used to improve manufacturing processes and can effectively distinguish controllable parameter levels in a manufacturing process. In the Taguchi method of parameter design, robustness concepts are used to improve the product performance and reduce manufacturing costs. In this study, we use an L9 orthogonal array to determine the relationships of the MFC power density with various EPD parameters. We selected the applied voltage (V), deposition time (s), deposition temperature (℃), and graphene concentration (wt%) as the control parameters. The control parameters and corresponding levels are listed in Table 1. We use the four control parameters with three levels to conduct parameter optimization. Table 2 shows the details of the orthogonal array design of the experimental parameters.

3. Results and Discussion

3.1 Polarization curves

Polarization curves are often used to assess the performance of MFCs. Through polarization curves, electrode voltage changes in response to a change in current density can be observed. In this study, we use an electrochemical analyzer to measure the voltage of the MFC electrode at the maximum power generation capacity. The resulting MFC voltages corresponding to different currents are plotted as a polarization curve. We use the Taguchi method to substitute crucial parameters affecting the EPD efficiency, with these parameters defined in an L9(3^4) orthogonal

Table 1
Experimental parameter levels.

Control parameter	Symbol	Level 1	Level 2	Level 3
Applied voltage (V)	A	5	15	20
Deposition time (s)	B	30	60	120
Deposition temperature (℃)	C	5	25	50
Graphene concentration (wt%)	D	0.01	0.02	0.03

Table 2
Orthogonal array.

Experiment no.	Applied voltage (V)	Deposition time (s)	Deposition temperature (°C)	Graphene concentration (wt%)
TM1	5	30	5	0.01
TM2	5	60	25	0.02
TM3	5	120	50	0.03
TM4	15	30	25	0.03
TM5	15	60	50	0.01
TM6	15	120	5	0.02
TM7	20	30	50	0.02
TM8	20	60	5	0.03
TM9	20	120	25	0.01

array, to generate nine manufacturing processes. An unmodified SSM is used as the control electrode. In the experiment, three electrochemical measurements are conducted for each MFC group. The power density curve of the MFC 8 h after its assembly is recorded.

3.2 Signal-to-noise ratio analysis

In the Taguchi method, the signal-to-noise (*SN*) ratio is used to measure quality. The calculation method is shown by Eqs. (1)–(4). Different quality characteristics were calculated on the basis of the nominal the best [Eq. (2)], smaller the better [Eq. (3)], and larger the better [Eq. (4)] characteristics.[24]

$$\frac{S}{N} = -10\log\left[MSD\right] \tag{1}$$

$$MSD = \frac{\sum_{i=1}^{n}(y_i - m)^2}{n} = \left(\overline{y} - m\right)^2 + S^2 \tag{2}$$

$$MSD = \frac{\sum_{i=1}^{n} y_i^{\,2}}{n} = \overline{y}^2 + S^2 \tag{3}$$

$$MSD = \frac{\sum_{i=1}^{n}(1/y_i)^2}{n} \tag{4}$$

Here, MSD is the mean squared error, $\overline{y}$ is the mean power density, and S is the standard deviation. The equations for $\overline{y}$ and S are

$$\bar{y} = \frac{\sum_{i=1}^{n} y_i}{n}, \tag{5}$$

$$S = \sqrt{\frac{\sum_{i=1}^{n} (y_i - \bar{y})^2}{n-1}}. \tag{6}$$

Because a larger MFC power density represents a higher overall power generation efficiency, the maximum power density was set as the experimental observation value. The larger the better equation [Eq. (4)] was used to calculate the *SN* ratio. The experimental results are presented in Table 3.

The initial power density following the completion of MFC assembly was unstable. In consideration of MFC stability and durability, in this study, we conducted an in-depth exploration of the data obtained from the MFC 8 h after the completion of assembly. Figure 3 shows the maximum power density at this time. N-8h represents the power density curve measured at the anode comprising the unmodified SSM; the maximum power density was 0.70 mW/m^2. TM5-8h is the power density curve measured at the MFC anode fabricated using the fifth group of EPD parameters in the Taguchi method; the maximum power density was 5.65 mW/m^2, approximately eightfold that for the unmodified SSM.

In this study, we use four parameters with three levels; thus, the L9(3^4) orthogonal array was used for the experiment. Because a higher MFC power density corresponds to a higher overall power generation efficiency, the maximum power density was set as the experimental observation value. The experimental results are recorded in Table 3. Once the *SN* ratio of each parameter combination had been calculated, factor response analysis was conducted and the results are plotted in the factor response curves shown in Fig. 4.

Table 3
Maximum power density SN ratios.

Experiment no.	Maximum power density			Average	*S*	*SN*
	*y*1	*y*2	*y*3			
TM1	1.031	0.945	1.701	1.226	0.414	0.9
TM2	0.819	1.757	1.734	1.437	0.535	1.5
TM3	0.656	0.768	0.514	0.646	0.127	−4.1
TM4	1.424	1.25	1.614	1.429	0.182	3.7
TM5	3.681	4.93	5.678	4.763	1.009	13.1
TM6	1.773	1.338	1.556	1.556	0.218	3.7
TM7	1.786	2.658	1.514	1.986	0.598	5.3
TM8	2.846	1.032	2.05	1.976	0.909	3.6
TM9	0.898	2.653	1.749	1.767	0.878	2.4

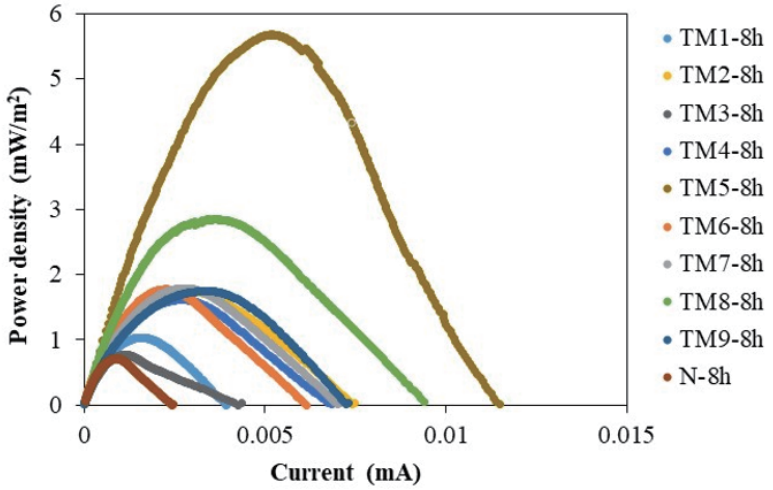

Fig. 3. (Color online) Maximum power density of the MFC 8 h after the completion of assembly.

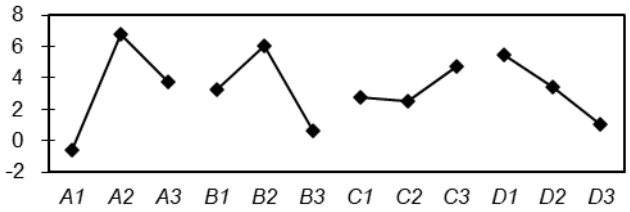

Fig. 4. Factor response curves obtained in the maximum power density experiment.

3.3 Analysis of variance

Standard deviation and sample size can be used to evaluate the confidence interval of each calculated value under given confidence levels. For example, the confidence interval under a 95% confidence level can be referred to as the 5% error. To further identify the effect of each factor on the MFC power generation efficiency, we conduct the analysis of variance (ANOVA) on the MFC maximum power density. From the ANOVA calculations, the vectors of the experimental factor variance were obtained.[24]

$$SS_T = \sum_{i=1}^{m} \eta_i^2 - \frac{1}{m}\left(\sum_{i=1}^{m} \eta_i\right)^2 \tag{7}$$

Here, m is the number of experiments in the orthogonal array and η_i is the average SN ratio of experiment i. The squared sum of the control parameter (SS_P) was defined as

$$SS_P = \sum_{j=1}^{t} \frac{\left(s\eta_j\right)^2}{t} - \frac{1}{m}\left(\sum_{i=1}^{m} \eta_i\right)^2, \tag{8}$$

where j is the number of factor levels, t is the number of repetitions of the levels of each factor, and $s\eta_i$ is the sum of the SN ratios for factor level j. The error sum of squares was calculated using

$$SS_e = \sum_{i=1}^{n} S_i^2 \times (r-1). \tag{9}$$

The degree of freedom of each control factor was DOF_P¼t_1. The total number of degrees of freedom was DOF_T¼m_1. The factor variance was V_P¼$SS_P = DOF_P$. The contribution percentage of each factor could be calculated as

$$P_P = \frac{SS_P - DOF_P \times V_e}{SS_T}. \tag{10}$$

According to Table 4, the EPD control factors that affected the MFC power density, from most to least strongly, were the deposition voltage (A), deposition time (B), graphene concentration (D), and suspension temperature (C). Factors A, B, and D satisfied the 99% confidence level and were thus critical factors affecting the MFC power density. Factor C only reached the 98.81% confidence level and had a smaller effect on the experiment; thus, it was classified as an error.

3.4 Confirmatory experiment

Once the optimal parameter combination had been obtained and ANOVA had been conducted, we compared the predicted and confirmatory values to verify the reliability of the optimization. The maximum power density was the main indicator of the MFC power generation efficiency. Through Eq. (11), the predicted SN ratio of the optimal EPD parameter conditions (η_{pre}) was calculated as 11.8 dB. The predicted optimal MFC maximum power density (η_{pre}) was 3.89 mW/m^2. The F value was 19.0. The 5% confidence interval result was 11.8 dB. The predicted and confirmatory values are summarized in Table 5. According to Table 5, the error between the predicted and confirmatory values of the maximum power density was 0.91 mW/

Table 4
ANOVA results for SN ratio in the maximum power density experiment.

Factor	*SS*	*DOF*	*Var*	*F*	Probability (%)	Confidence (%)	Significant*
A	10.551	2	5.275	13.27	0.03	99.97	Yes
B	9.905	2	4.952	12.46	0.04	99.96	Yes
C	4.555	2	2.278	5.73	1.19	98.81	No
D	6.932	2	3.466	8.72	0.22	99.78	Yes
Error	7.155	18	0.398	S = 0.630			
Total	39.1	26	1.503				

*At least 99% confidence level.

Table 5
Predicted and confirmatory values of the maximum power density.

Confirmatory values		Predicted values		Differences	
$P_{are}\left(\frac{mW}{m^2}\right)$	η_{conf} (dB)	$P_{pre}\left(\frac{mW}{m^2}\right)$	η_{pre} (dB)	$\lvert P_{are} - P_{pre}\rvert$	$\lvert \eta_{conf} - \eta_{pre}\rvert$
4.8	13.1	3.89	11.8	0.91	1.3

m^2. The error between the predicted and confirmatory values of the *SN* ratio was 1.3 dB, lower than the 3.5 dB of the 5% confidence interval calculated using Eq. (12). The calculation results confirmed that the experimental results satisfied the 95% confidence level.

$$\eta_{pre} = \overline{\eta} + \left(\overline{A_i} - \overline{\eta}\right) + \left(\overline{B_j} - \overline{\eta}\right) + \left(\overline{C_k} - \overline{\eta}\right) + \cdots \tag{11}$$

$$CI = \sqrt{F_{0.05,2,\nu_y} \times V_e \times \left(\frac{1+\nu}{n_{tol}} + \frac{i}{n_{conf}}\right)} \tag{12}$$

3.5 Anode surface scanning electron microscopy

In this study, we perform scanning electron microscopy (SEM) to observe the difference in the morphology of the surface of the unmodified SSM and the SSMs modified using EPD parameters in accordance with the Taguchi orthogonal array [L9(3^4) array]. Figure 4 shows an image of the unmodified SSM, where (a) and (b) respectively show the image under 150× and 1500× magnification. The unmodified SSM had a smooth surface morphology. Figures 5–14 present SEM images of the anodes fabricated using the first to ninth groups of fabrication conditions, respectively. Under the first group of conditions, the graphene deposition was uneven and small in amount, whereas under the second group of fabrication conditions, more graphene was deposited on the surface and the graphene was more evenly distributed. Under the third group of fabrication conditions, the graphene on the electrode surface was dense, and aggregation could be observed at the intersections between SSM wires. Under the fourth group of fabrication conditions, the graphene distribution was relatively even. Under the fifth group of fabrication conditions, the surface graphene distribution was again relatively even but also without notable aggregation. Under the sixth group of fabrication conditions, the graphene was dense on the surface but uneven with notable aggregation. Under the seventh group of fabrication conditions, the deposited graphene was dense and even. Under the eighth group of fabrication conditions, the deposited graphene was again dense and even, but aggregation was observed at some wire intersections in the SSM. Finally, under the ninth group of fabrication conditions, the graphene was found to be distributed unevenly with notable aggregation. The different MFC power densities may have been due to the differing SSM surface morphologies resulting from the different EPD parameters.

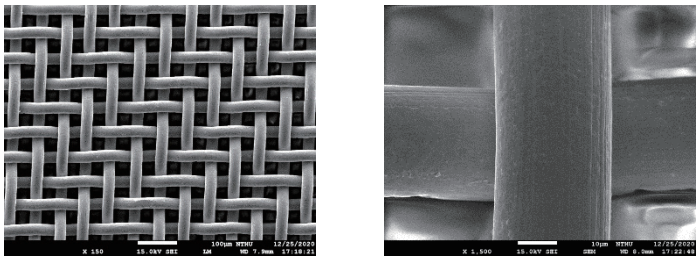

(a) (b)

Fig. 5. SEM images of the unmodified SSM at different magnifications: (a) 150× and (b) 1500×.

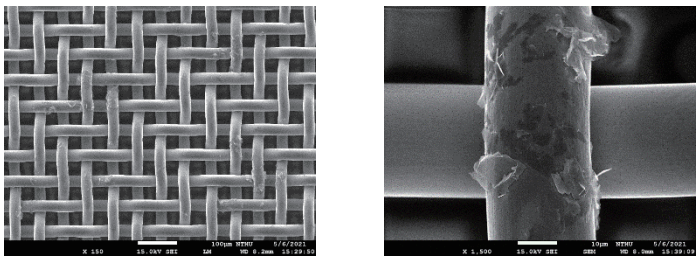

(a) (b)

Fig. 6. SEM images of the SSM anode fabricated using the first Taguchi group of parameters at different magnifications: (a) 150× and (b) 1500×.

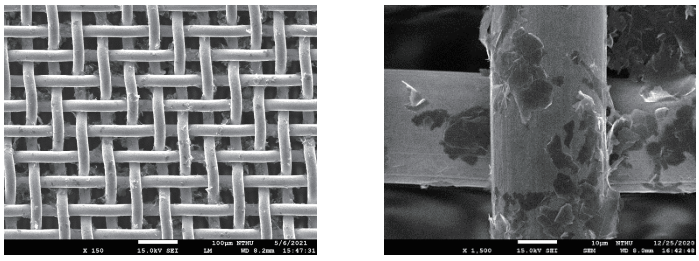

(a) (b)

Fig. 7. SEM images of the SSM anode fabricated using the second Taguchi group of parameters at different magnifications: (a) 150× and (b) 1500×.

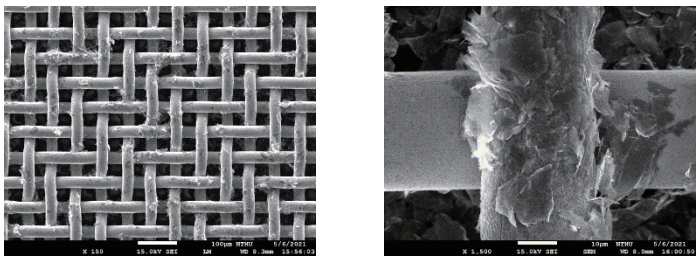

(a) (b)

Fig. 8. SEM images of the SSM anode fabricated using the third Taguchi group of parameters at different magnifications: (a) 150× and (b) 1500×.

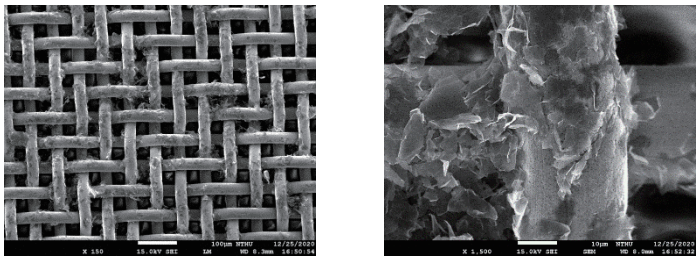

(a) (b)

Fig. 9. SEM images of the SSM anode fabricated using the fourth Taguchi group of parameters at different magnifications: (a) 150× and (b) 1500×.

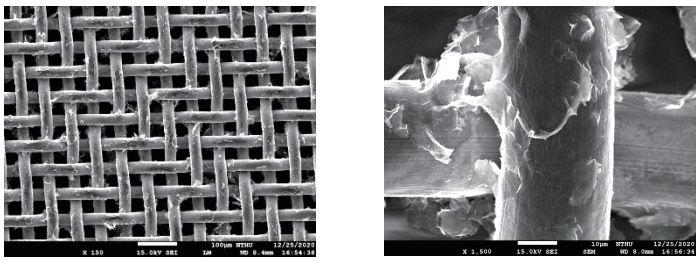

(a) (b)

Fig. 10. SEM images of the SSM anode fabricated using the fifth Taguchi group of parameters at different magnifications: (a) 150× and (b) 1500×.

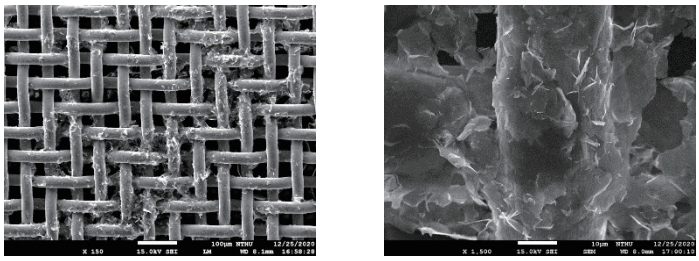

(a) (b)

Fig. 11. SEM images of the SSM anode fabricated using the sixth Taguchi group of parameters at different magnifications: (a) 150× and (b) 1500×.

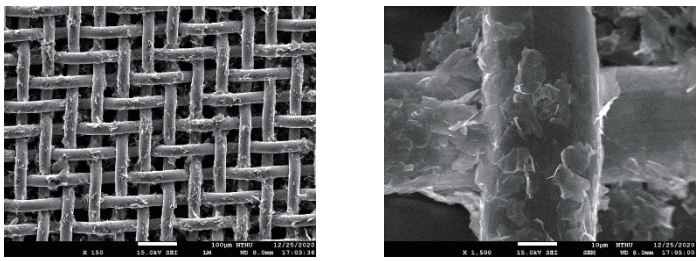

(a) (b)

Fig. 12. SEM images of the SSM anode fabricated using the seventh Taguchi group of parameters at different magnifications: (a) 150× and (b) 1500×.

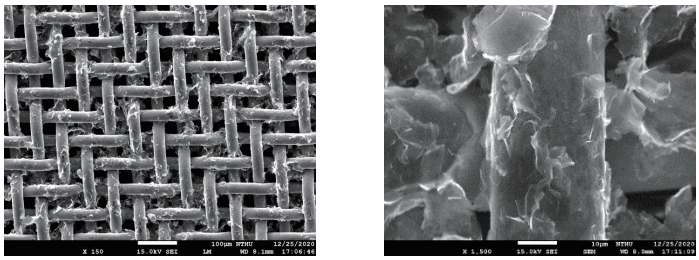

(a) (b)

Fig. 13. SEM images of the SSM anode fabricated using the eighth Taguchi group of parameters at different magnifications: (a) 150× and (b) 1500×.

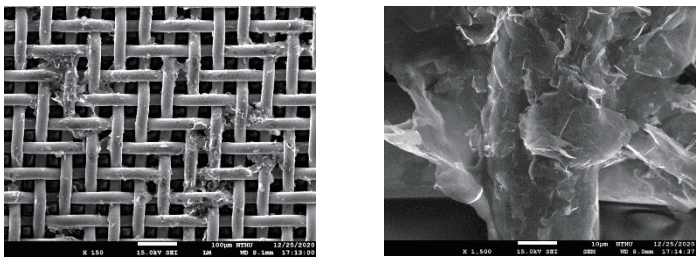

(a) (b)

Fig. 14. SEM images of the SSM anode fabricated using the ninth Taguchi group of parameters at different magnifications: (a) 150× and (b) 1500×.

4. Conclusions

This study was focused on energy harvester technology, specifically the micro/nanostructure fabrication of nanomaterials used for anode electrodes in energy collection. In this research, a graphene suspension was prepared by mixing graphene powder with deionized water in a 1:1 ratio and adding 95% ethanol. EPD was then used to form a uniform graphene coating on the surface of an SSM anode. During the EPD process, oxygen-containing functional groups on the graphene surface were reduced to carbon ring structures, enhancing the material's conductivity, surface area, and electrochemical activity. These micro/nanostructural improvements significantly contributed to the enhanced energy harvesting performance of the MFC, as demonstrated by the increased power output. The results of this work highlight the potential of integrating nanomaterials and micro/nanofabrication techniques in the development of efficient energy harvesting systems.

Numerous factors can affect EPD efficiency. We used the Taguchi method to optimize the EPD process and selected four parameters that had substantial effects on the EPD efficiency, namely, graphene concentration, deposition time, applied voltage, and suspension temperature. For each parameter, three levels were applied in an L9(3^4) orthogonal array. A total of nine parameter combinations were thus employed in the experiment. To ensure the reliability of the experimental results, each group was tested three times and the Taguchi method was used to analyze the experimental data. Below are the details of the conclusions of the present study.

- EPD has the advantages of easy installation, a simple process, and convenience for mass production. We used EPD to fabricate a graphene-covered SSM for use as an MFC anode to improve the MFC's power generation efficiency and reduce the cost of graphene electrode fabrication.
- The Taguchi method was employed to optimize the EPD process parameters; 81 groups of experiments were effectively integrated into nine groups. The experimental results of the Taguchi method revealed that the EPD parameters, ranked from most to least important in terms of their effect on the MFC power density, were applied voltage (A), deposition time (B), graphene concentration (D), and suspension temperature (C). Graphene concentration was the most critical factor affecting the MFC oxidation peak current.
- In the Taguchi experiment regarding the maximum power density, the optimal parameter combination was A2B2C3D1, matching the fifth group in the orthogonal array. The error between the predicted and confirmatory values was 1.3 dB, which is lower than the 3.5 dB of the 5% confidence interval calculated using Eq. (12). The experimental results satisfied the 95% confidence level, and the maximum power density was eightfold that for the unmodified anode.

References

1 M. F. Demirbas, M. Balat, and H. Balat: Energ. Convers. Manage. **50** (2009) 1746. https://doi.org/10.1016/j.enconman.2009.03.013
2 A. K. Shukla, P. Suresh, B. Sheela, and A. J. C. S. Rajendran: Curr. Sci. **87** (2004) 455. https://repository.ias.ac.in/81820/
3 W. Grzebisz, L. Ciesla, J. Komisarek, and J. Potarzycki: Pol. J. Environ. Stud. **11** (2002) 493. https://www.pjoes.com/pdf-87482-21341
4 H. Ren, S. Pyo, J. I. Lee, T. J. Park, F. S. Gittleson, F. C.C. Leung, J. Kim, A. D. Taylor, H. S. Lee, and J. Chae: J. Power Sourc. **273** (2015) 823. https://doi.org/10.1016/j.jpowsour.2014.09.165
5 C. Erbay, X. Pu, W. Choi, M. J. Choi, Y. Ryu, H. Hou, F. Lin, P. de Figueiredo, C. Yu, and A. Han: J. Power Sourc. **280** (2015) 347. https://doi.org/10.1016/j.jpowsour.2015.01.065
6 W. H. Hsu, H. Y. Tsai, and Y. C. Huang: J. Nanomater. **2017** (2017) 9875301. https://doi.org/10.1155/2017/9875301
7 H. Y. Tsai, W. H. Hsu, and M. Z. You: Mach. Sci. Technol. **26** (2022) 1003. https://doi.org/10.1080/10910344.2023.2181088
8 S. F. Ketep, A. Bergel, A. Calmet, B. Erable: Energy Environ. Sci. **7** (2014) 1633. https://doi.org/10.1039/C3EE44114H
9 K. Guo, A. H. Soeriyadi, H. Feng, A. Prévoteau, S. A. Patil, J. J. Gooding, and K. Rabaey: Bioresour. Technol. **195** (2015) 46. https://doi.org/10.1016/j.biortech.2015.06.060
10 Z. Qiu, L. Wei, G. Wang, M. Su, and J. Shen: RSC Advances **5** (2015) 46210. https://doi.org/10.1039/C5RA06448A
11 J. Hou, Z. Liu, Y. Li, S. Yang, and Y. Zhou: Bioprocess Biosyst. Eng. **38** (2014) 881. https://doi.org/10.1007/s00449-014-1332-0
12 J. Hou, Z. Liu, S. Yang, and Y. Zhou: J. Power Sourc. **258** (2015) 204. https://doi.org/10.1016/j.jpowsour.2014.02.035
13 H. M. Cho, H. Ha, and Y. Ahn: ACS Sustain. Chem. Eng. **10** (2022) 1839. https://doi.org/10.1021/acssuschemeng.1c07011
14 E. T. Sayed, H. Alawadhi, A. G. Olabi, A. Jamal, M. S. Almahdi, J. Khalid, and M. A. Abdelkareem: Int. J. Hydrog. Energ. **46** (2021) 5975. https://doi.org/10.1016/j.ijhydene.2020.10.043
15 Y. J. Choi, H. O. Mohamed, S. G. Park, R. B. Al Mayyahi, M. Al-Dhaifallah, H. Rezk, X. Ren, H. Yu, and K. J. Chae: Int. J. Hydrog. Energ. **45** (2020) 5960. https://doi.org/10.1016/j.ijhydene.2019.05.091
16 R. T. Khajeh, S. Aber, and K. Nofouzi: Mater. Chem. Phys. **240** (2020) 122208. https://doi.org/10.1016/j.matchemphys.2019.122208

17 N. N. M. Noor, R. Misali, M. Kim, J. Park, M. Ko, I. C. Lee, T. Hibino, and K. Kim: J. Taiwan Inst. Chem. Engrs. **168** (2025) 105929. https://doi.org/10.1016/j.jtice.2024.105929
18 W. M. A. Abbas, and Z. Z. Ismail: J. Power Sourc. **628** (2025) 235927. https://doi.org/10.1016/j.jpowsour.2024.235927
19 H. Y. Tsai, W. H. Hsu, and Y. J. Liao: Coatings **8** (2018) 243. https://doi.org/10.3390/coatings8070243
20 P. Sarkar and P. S. Nicholson: J. Am. Ceram. Soc. **79** (1996) 1987. https://doi.org/10.1111/j.1151-2916.1996.tb08929.x
21 M. Atiq Ur Rehman, Q. Chen, A. Braem, M. S. Shaffer, and A. R. Boccaccini: Int. Mater. Rev. **66** (2021) 533. https://doi.org/10.1080/09506608.2020.1831299
22 S. J. An, Y. Zhu, S. H. Lee, M. D. Stoller, T. Emilsson, S. Park, and R. S. Ruoff: J. Phys. Chem. Lett. **1** (2010) 1259. https://doi.org/10.1021/jz100080c
23 M. Rahimnejad, G. D. Najafpour, A. A. Ghoreyshi, M. Shakeri, and H. Zare: Int. J. Hydrogen. Energ. **36** (2011) 13335. https://doi.org/10.1016/j.ijhydene.2011.07.059
24 Y. H. Guu, C. S. Deng, M. T. K. Hou, C. H. Hsu, and K. S. Tseng: Mater. Manuf. Process. **27** (2012) 207. https://doi.org/10.1080/10426914.2011.566657

About the Authors

Wei-Hsuan Hsu earned his B.S. degree from National Central University in Taiwan in 2004, followed by his M.S. and Ph.D. degrees from National Tsing Hua University in 2006 and 2012, respectively. He served as an assistant professor at National United University from 2013 to 2016 and has been an associate professor there since 2017. His research interests include optical measurement and ultraprecision machining technologies.
(whhsu@nuu.edu.tw)

Zih-Yu Lin received her B.S. and M.S. degrees from National United University, Taiwan, in 2017 and 2020, respectively. Her research interests are in microbial fuel cells and electrophoretic deposition. (stu910327@gmail.com)